Available online at www.sciencedirect.com
ScienceDirect
European Journal of Medicinal Chemistry 44 (2009) 212–228
EUROPEAN JOURNAL OF MEDICINAL CHEMISTRY
http://www.elsevier.com/locate/ejmech

Original article

Penetratin and derivatives acting as antifungal agents

Marcelo F. Masman [a,b,c], Ana M. Rodríguez [a,b], Marcela Raimondi [d], Susana A. Zacchino [e], Paul G.M. Luiten [c], Csaba Somlai [f], Tamas Kortvelyesi [g], Botond Penke [f], Ricardo D. Enriz [a,b,*]

[a] *Facultad de Química, Bioquímica y Farmacia, Universidad Nacional de San Luis, Chacabuco 915, 5700 San Luis, Argentina*
[b] *IMBIO-SL, CONICET, UNSL, Chacabuco 915, 5700 San Luis, Argentina*
[c] *Department of Molecular Neurobiology, Centre for Behaviour and Neurosciences, University of Groningen, Kerklaan 30, 9751 NN Haren, The Netherlands*
[d] *Microbiología, Facultad de Medicina, Universidad Nacional de Rosario, Santa Fe 3100, 2000 Rosario, Argentina*
[e] *Farmacognosia, Facultad de Ciencias Bioquímicas y Farmacéuticas, Universidad Nacional de Rosario, Suipacha 531, 2000 Rosario, Argentina*
[f] *Department of Medical Chemistry, University of Szeged, Dóm ter 8, H-6720 Szeged, Hungary*
[g] *Department of Physical Chemistry, University of Szeged, Rerrich Sq. 1, H-6720 Szeged, Hungary*

Received 26 December 2007; received in revised form 8 February 2008; accepted 11 February 2008
Available online 29 February 2008

Abstract

The synthesis, in vitro evaluation, and conformational study of RQIKIWFQNRRMKWKK–NH_2 (penetratin) and related derivatives acting as antifungal agents are reported. Penetratin and some of its derivatives displayed antifungal activity against the human opportunistic pathogenic standardized ATCC strains *Candida albicans* and *Cryptococcus neoformans* as well as clinical isolates of *C. neoformans*. Among the compounds tested, penetratin along with the nonapeptide RKWRRKWKK–NH_2 and the tetrapeptide RQKK–NH_2 exhibited significant antifungal activities against the *Cryptococcus* species. A comprehensive conformational analysis on the peptides reported here using three different approaches, molecular mechanics, simulated annealing and molecular dynamics simulations, was carried out. The experimental and theoretical results allow us to identify a topographical template which may provide a guide for the design of new compounds with antifungal characteristics against *C. neoformans*.

Keywords: Penetratin; Cationic peptides; Cryptococcosis; *Candida* infections; Molecular dynamics; Conformational analysis

1. Introduction

Fungal infections are a persistent major health problem, which especially affect and threaten immunocompromised patients [1,2]. Invasive fungal infections as well as dermatomycoses produced by fungal organisms with even low virulence can be life threatening [3] for individuals with increased vulnerability such as neonates, cancer patients receiving chemotherapy, organ transplant patients, and burns patients, apart from those with acquired immunodeficiency syndrome (AIDS). Other risk factors include corticosteroid and antibiotic treatments, diabetes, lesions of epidermis and dermis, malnutrition, neutropenia and surgery [2]. Many fungal infections are caused by opportunistic pathogens that may be endogenous or acquired from the environment (*Candida*, *Cryptococcus*, *Aspergillus* infections). Patients with significant immunosuppression frequently develop *Candida* esophagitis. Cryptococcosis, caused by the encapsulated yeast *Cryptococcus neoformans*, has been the cause of fungal

Abbreviations: AIDS, acquired immunodeficiency syndrome; CPP, cell-penetrating peptide; SA, simulated annealing; MD, molecular dynamics; MIC, minimum inhibitory concentration; MFC, minimum fungicide concentration; EDMC, electrostatically driven Monte Carlo; RMSD, route mean square deviation; R_g, radius of gyration; RMSF, root mean square fluctuation; SASA, solvent accessible surface area; TFE_{d2}, trifluoroethanol-d_2; MEPs, molecular electrostatic potentials.

* Corresponding author. Facultad de Química, Bioquímica y Farmacia, Universidad Nacional de San Luis, Chacabuco 915, 5700 San Luis, Argentina. Tel.: +54 2652 423789; fax: +54 2652 431301.
E-mail address: denriz@unsl.edu.ar (R.D. Enriz).

0223-5234/$ - see front matter © 2008 Elsevier Masson SAS. All rights reserved.
doi:10.1016/j.ejmech.2008.02.019

mortality among HIV-infected patients. This organism has a predilection for the central nervous system and leads to severe, life-threatening meningitis. In addition, an increasing number of normal individuals, including children in third-world nations [4] that suffer deficient sanitation and education, are prone to fungal infections, especially those involving the skin and mucosal surfaces.

Although it appears that many drugs are available for the treatment of systemic and superficial mycoses, there are in fact only a limited number of effective antifungal drugs [1]. Many of the antifungal compounds currently available have undesirable effects or are very toxic (amphotericin B); are fungistatic and not fungicidal (azoles), or lead to the development of resistance, as with 5-fluorocytosine [5]. Amphotericin B, developed in the 1950s, still remains as a widely used antifungal drug, most recently gaining renewed applications through lipid based formulations. According to Polak [6] ideal drugs to cure fungal infections have not been discovered yet. In the meantime, resistance to currently available antifungal agents continues to grow [7]. Although combination therapy has emerged as a good alternative to bypass these disadvantages [6,8], there is an urgent need for a next generation of safer and more potent antifungal agents [1,8]. These explorations have resulted in the identification of novel molecules, which could prove promising for further future development. Among them, some natural peptides were recently described as antifungal compounds, inhibiting a broad spectrum of fungi [9–11]. It has also been reported that a group of cationic antimicrobial peptides are major players in the innate immune response [12,13]. These peptides are very ancient elements of the immune response of all species of animal and plant life, and the induction pathways for these compounds in vertebrates, insects and plants [12–14] are highly conserved. Furthermore, it is becoming increasingly clear that cationic antimicrobial peptides play many potential roles in inflammatory responses, which represent an orchestration of the mechanisms of innate immunity.

Small cationic peptides [15,16] are abundant in nature and have been described as ''nature's antibiotics'' or ''cationic antimicrobial peptides''. These peptides are 12–50 amino acids long with a net positive charge of +2 or +9, which is due to an excess of basic arginine and lysine residues, and approximately 50% hydrophobic amino acids [15]. These molecules are also folded in three dimensions so that they have both a hydrophobic face comprising non-polar amino acid side chains, and a hydrophilic face of polar and positively charged residues: these molecules are amphipathic. Despite these two similarities these compounds vary considerably in length, amino acid sequence and secondary structure. The different spatial orderings include small β-sheets stabilized by disulphide bridges, amphipathic α-helices and, less commonly, extended and loop structures.

Cell-penetrating peptides (CPPs) are defined as peptides with a maximum of 30 amino acids, which are able to enter cells in a seemingly energy-independent manner, thus being able to translocate across membranes in a non-endocytotic fashion [17]. In 1991, Joliot et al. [18] reported that the 60 amino acid homeodomain of the Antennapedia protein of *Drosophila* was able to translocate over cell membranes. In order to understand the driving force for the internalization, the homeodomain was modified by site-directed mutagenesis leading to the discovery that its third helix was necessary and also sufficient for membrane translocation, which resulted in the development of a 16 amino acid-long CPP called penetratin (**1**) [19]. Thus, peptide **1**, a synthetic 16 amino acid peptide from the third helix of Antennapedia homeodomain [19,20], is a cationic amphipathic peptide which might penetrate cell membranes *via* a proposed ''inverted micelle'' pathway. However, the mechanism of membrane translocation is not well known. The question is whether the peptide is internalized *via* endocytosis which is energy-dependent or *via* direct transport, while the latter mechanism is scarcely known at present, it is believed that the process is non-receptor mediated [20,21]. In addition, we previously provide evidence on the energy-dependent and lipid raft-mediated endocytic uptake of penetratin [22]. Peptide **1** has been proposed as a universal intracellular delivery vehicle [23]. Since **1** possesses 16 amino acids and a charge of +8, it might be included in the general classification of ''cationic antimicrobial peptide''. To the best of our knowledge this is the first study reporting the antifungal activity of **1** and structurally related derivatives.

The aim of the present investigation is exploring the antifungal potential of **1** and its derivatives against *Candida albicans* and *C. neoformans*. To better characterize the structure–antifungal activity relationship of peptide **1** and related compounds under study the present analysis explored influences of amino acid substitutions and deletions on its antifungal activity. In addition, an extensive conformational analysis of **1** and its derivatives was carried out using three different approaches: molecular mechanics, simulated annealing (SA) and molecular dynamics (MD) simulations. The ability of each method to obtain the different conformations is tested and compared. Conformational and electronic studies were carried out in order to identify a topographical and/or a sub-structural template, which may be the starting structure for the design of new antifungal compounds.

2. Results and discussion

2.1. Antifungal activity

To evaluate the antifungal potential, concentrations of peptides up to 200 μM were incorporated in the growth media according to previously reported procedures [11,24,25]. Compounds producing no inhibition of fungal growth at 200 μM were considered inactive. Table 1 gives the antifungal activity obtained for peptide **1** against *C. albicans* and *C. neoformans*. Peptide **1** displayed a significant antifungal activity against both fungi being *C. neoformans* the more sensitive species. It is interesting to note that **1** displayed a significant degree of inhibition against *C. neoformans* even at low concentrations (90% of inhibition was observed at 12.5 μM and 100% at 25 μM). The inhibitory effect observed against *C. albicans*

Table 1
Antifungal activity (% inhibition) of peptides against *Candida albicans* ATCC 10231 and *Cryptococcus neoformans* ATCC 32264 (% of inhibitions higher than 60 are shown in bold)

Peptide	Sequence	*Candida albicans*					*Cryptococcus neoformans*				
		200 μM	100 μM	50 μM	25 μM	12.5 μM	200 μM	100 μM	50 μM	25 μM	12.5 μM
1	RQIKIWFQNRRMKWKK–NH_2	**100** ± 0.2	**100** ± 0.6	**95** ± 1.2	**91** ± 1.6	4 ± 0.1	**100** ± 0.1	**100** ± 0	**100** ± 0	**100** ± 0.2	**90** ± 2.3
2	WKQKNIKWRFRQKMIR–NH_2	60 ± 4.2	52 ± 3.0	0	0	0	**96** ± 2.7	**92** ± 5.7	36 ± 3.4	28 ± 2.9	0
3	RKWRRKWKK–NH_2	**100** ± 0.08	**76** ± 0.97	58 ± 0.71	40 ± 1.75	15 ± 1.0	**99** ± 1.68	**68** ± 21.22	14 ± 1.32	16 ± 1.78	0
4	RKFRRKFKK–NH_2	**61** ± 1.16	44 ± 7.00	33 ± 7.42	23 ± 3.79	0	**73** ± 1.51	11 ± 3.92	13 ± 2.32	9 ± 3.80	0
5	RKRRKWKK–NH_2	29 ± 1.05	13 ± 0.55	0	0	0	**100** ± 0.36	33 ± 4.79	11 ± 4.35	6 ± 2.14	0
6	RKRRKKK–NH_2	43 ± 4.96	12 ± 0.4	0	0	0	60 ± 2.94	14 ± 2.09	19 ± 6.73	10 ± 2.89	0
7	KWKK–NH_2	9 ± 2.3	2 ± 1.0	0	0	0	0	0	0	0	0
8	RQKK–NH_2	6 ± 1.2	0	0	0	0	**100** ± 1.2	**100** ± 4.0	**92** ± 3.6	**62** ± 7.4	32 ± 2.3
Amph. B[a]		100		100	100	100	100	100	100	100	100
Ket.[b]		100		100	100	100	100	100	100	100	100

[a] Amphotericin B.
[b] Ketoconazole.

was slightly lower than that obtained for *C. neoformans* at 12.5 μM but similar at 25–200 μM.

In order to gain insight into the spectrum of activity, peptide **1** was tested against a panel of clinical isolates of *C. neoformans*. The minimum inhibitory concentration (MIC) values of **1** were determined against this new panel by using three endpoints: MIC_{100}, MIC_{80} and MIC_{50} (the minimum concentration of compounds that inhibit 100, 80 and 50% of growth, respectively). The application of a less stringent end point such as MIC_{80} and MIC_{50} has been shown to consistently represent the in vitro activity of compounds and many times provide a better correlation with other measurements of antifungal activity such as the minimum fungicide concentration (MFC) [26]. In addition to MIC determinations, the evaluation of MFC of **1** against this panel was accomplished by sub-culturing a sample of media from MIC tubes showing no growth, onto drug-free agar plates. So, peptide **1** was tested against 10 clinical isolates of *C. neoformans*, all provided by the Malbrán Institute (Buenos Aires). These results are shown in Table 2 and the activity was similar to, or lower than, those obtained against the standard strain (ATCC 32264).

Peptide **2** possesses the same amino acids of peptide **1** but located in a completely different sequence. In fact, the sequence of this peptide was randomly generated. This peptide showed no antifungal activity against both fungi tested at 12.5 μM but inhibited 96 and 60% of the growth of *C. neoformans* and of *C. albicans* at 200 μM, respectively. It is clear that the antifungal activity of **1** and **2** is markedly different, whereas **1** showed a significant antifungal activity against both *C. albicans* and *C. neoformans*; peptide **2** was practically inactive. On the basis of these results it can be concluded that the sequence as well as the different spatial orderings of the cationic, polar and hydrophobic residues are important determinants for the antifungal activity. In contrast, the positive charge (+8) of **1** appears to be a necessary requirement but not by itself sufficient to produce the antifungal response.

To study the structure–antifungal activity relationship on these peptides, the effects of structural changes in the

Table 2
Minimum inhibitory concentrations (MIC_{100}, MIC_{80} and MIC_{50}) and minimum fungicidal concentration (MFC) of penetratin (**1**) against clinical isolates of *C. neoformans*

Voucher specimen	MIC_{100}	MIC_{80}	MIC_{50}	MFC	Amph. B MIC_{100}	Itz. MIC_{100}
IM 983040	31.2	31.2	31.2	31.2	0.13	<0.015
IM 972724	62.5	62.5	31.2	62.5	0.06	0.25
IM 042074	62.5	62.5	31.2	62.5	0.25	<0.015
IM 983036	62.5	62.5	31.2	62.5	0.13	<0.015
IM 00319	62.5	62.5	31.2	62.5	0.25	<0.015
IM 972751	62.5	31.2	31.2	62.5	0.25	<0.015
IM 031631	62.5	31.2	16	62.5	0.13	0.25
IM 031706	125	31.2	16	125	0.25	0.50
IM 961951	125	31.2	16	125	0.06	<0.015
IM 052470	125	31.2	31.2	125	0.50	<0.015

MIC_{100}, MIC_{80} and MIC_{50}: concentration of a compound that caused 100, 80 or 50% reduction of the growth control, respectively. Within voucher specimen: IM = Malbran Institute (Buenos Aires, Argentina); Amph. B = amphotericin B; Itz. = itraconazole.

sequence of peptide **1** were considered. Our principal goal was to synthesize shorter derivatives of **1** trying to maintain the antifungal activity as much as possible. In the first step we synthesized compound **3**, a nonapeptide possessing the last four amino acids of **1**. In this peptide we maintain the same numbers of cationic amino acids (Arg and Lys) deleting Gln-2, Ile-3, Ile-5, Phe-7, Gln-8, Asn-9 and Asn-12. Peptide **3** displayed a lower antifungal activity with respect to **1**. The antifungal activity against *C. neoformans* and *C. albicans* was moderately effective but still significant. We decided to perform changes on peptide **3** and then we synthesized peptides **4**–**6**. In peptide **4** we replaced the two Trp residues of peptide **3** (Trp-3 and Trp-7) by Phe. This structural change yielded a reduction of antifungal activity (compare the % of inhibition of **3** and **4** in Table 1), which is not an unexpected result; a role for Trp as translocation determinant of peptides has been proposed [27] and mutation of both tryptophans in peptide **1** was found to abolish internalization [19]. In addition, it has previously been reported that tryptophans are poorly replaceable by phenylalanine in **1** and derivatives when tested for their penetrating properties [28]. Our results lend support to previously reported findings, but in addition demonstrate the antifungal activity of these peptides. Octapeptide **5** was obtained by deleting Trp-3 from peptide **3**; in turn heptapeptide **6** was obtained by deleting Trp-3 and Trp-7 from peptide **3**. Whereas octapeptide **5** displayed only a marginal antifungal activity, peptide **6** was practically ineffective in comparison to their congeners.

In order to further understand the above experimental results, we performed a conformational study of the peptides reported here using different approaches.

2.2. Conformational study of peptide *1* and derivatives

A large number of studies have been performed in order to shed light on the structural aspects and mechanism of action for translocation of **1**. However, compared to these mechanistic properties, the conformational intricacies of this compound have received relatively little attention. It is, however, obvious that a better understanding of the conformational behavior of peptide **1** is of paramount importance. Linear peptides are highly flexible and therefore to determine the biologically relevant conformations is a matter of high complexity, which requires an exhaustive conformational analysis of these structures. Consequently, we carried out calculations using three different approaches: electrostatically driven Monte Carlo (EDMC) calculations implemented in the ECCEPAK [29] package, SA calculations using the Tinker Molecular Modelling package [30] and MD simulations from the GROMACS program [31,32].

2.2.1. EDMC results

EDMC results are summarized in Table 3 and Fig. 1 and more details are given in Tables SI–SVIII in Supplementary material. Calculations yielded a large set of conformational families for each peptide studied. The total number of conformations generated for each peptide varied between 47 391 and 129 922, and the number of those accepted was 5000 for all the cases. In the clustering procedure, an RMSD (root mean square deviation) of 0.75 Å and a cutoff of 30 kcal mol^{-1} were used. The number of families after clustering varied between 137 and 1001. The total number of families accepted with a relative population higher than 0.20% varied between 11 and 86. Their populations sum up to *ca.* 80% of all conformations in each case (see Table 3).

All low-energy conformers of the peptides studied here were then compared to each other. The comparison involved the spatial arrangements, relative energy and populations.

A total of 639 different families were found for peptide **1**. However, 82.92% of total population of this peptide corresponded to only 11 families (Table 3). It is interesting to note that the energetically preferred family comprises 70.48% of the entire population. Thus, this family which adopts an α-helix structure is the most representative form of this molecule. This conformation is characterized by stabilizing hydrogen bonds between the carbonylic oxygen (residue *i*) and the NH group (residue $i+4$). The first and the last residues do not present a stable structure. A spatial view of this conformation is shown in Fig. 1a. The second most populated family (7.46%) corresponds to a structure possessing the first

Table 3
Selected conformational search and clustering results for peptides **1**–**8** optimized at the EDMC/SRFOPT/ECCEP/3 level of theory

Peptide	Generated[a]				Accepted[b]				# F[c]	# $F_{0.20\%}$[d]	% P[e]
	Electrostatical	Random	Thermal	Total	Electrostatical	Random	Thermal	Total			
1	8973	119 535	575	129 083	1431	3245	324	5000	639	11	82.92
2	9200	120 229	493	129 922	1349	3373	278	5000	703	19	81.92
3	8050	107 710	304	116 064	1372	3412	216	5000	270	6	88.94
4	7490	102 380	245	110 115	1121	3697	182	5000	288	11	88.72
5	7905	106 150	294	114 349	1176	3606	218	5000	242	11	89.76
6	7191	98 483	213	105 887	1192	3635	173	5000	137	6	91.02
7	3007	44 352	32	47 391	508	4466	26	5000	505	74	82.82
8	3939	54 133	54	58 126	579	4379	42	5000	481	45	83.34

[a] Number of conformations generated electrostatically, randomly and thermally during the conformational search.
[b] Number of conformations accepted from those generated electrostatically, randomly and thermally during the conformational search.
[c] # F represents the total number of conformational families as result of the clustering run.
[d] # $F_{0.20\%}$ represents the number of conformational families with populations above 0.20%.
[e] % P represents the sum of the percent relative population of # $F_{0.20\%}$.

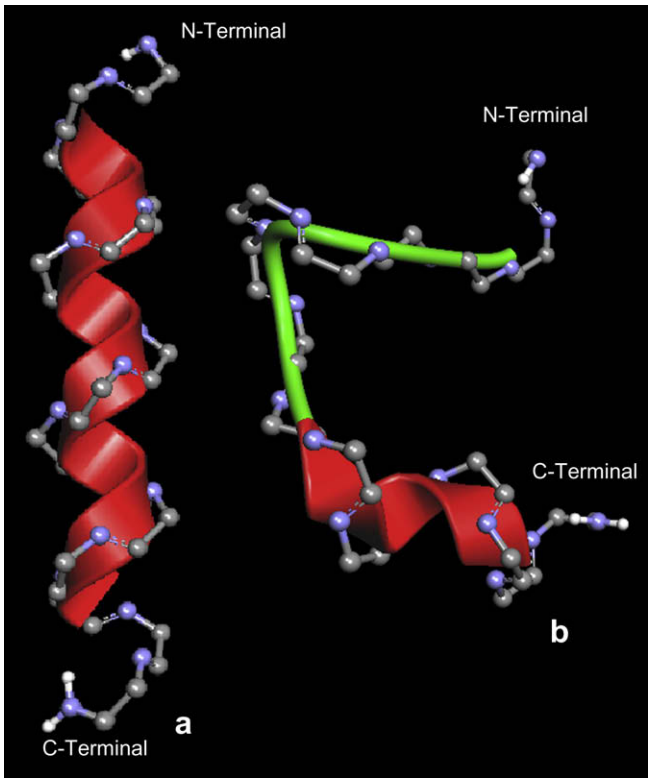

Fig. 1. Spatial view of the preferred forms obtained for peptide **1**. (a) The global minimum (α-helix structure) and (b) the second more populated conformation.

four residues without a stable structure; residues 5–7 in a turn structure and residues 10–15 with a typical α-helix structure. The residues 8 and 9 present a bend structure connecting the turn moiety with the α-helix portion. The last residue does not display a stable form (Fig. 1b). However, this family has an energy gap of 22.61 kcal mol^{-1} with respect to the global minimum.

For peptide **2** a total of 703 different families were obtained, from which 19 families comprise 81.92% of the total population. The most populated family (61.06%) presents an α-helix conformation from residues 3 to 15. This conformation has an energy gap of 1.27 kcal mol^{-1} with respect to the global minimum, which has 6.04% of population. The lowest energy conformation possesses the following structure: from residues 2 to 5 in a turn structure; residue 6 in a bend form and from residues 7 to 15 in a typical α-helix structure. Residues 1 and 16 do not show any stable structure. In general the conformational behavior of **1** and **2** is comparable. However, in peptide **1** the most populated family (a typical α-helix structure) is also the energetically preferred one. In contrast, for peptide **2**, the fully α-helix structure is not the most preferred form.

Compounds **3–6** display a closely related conformational behavior preferring a helical structure for the most populated families. Peptides **3–6** are somewhat more rigid with respect to **1**. This fact might be appreciated comparing the total number of conformational families obtained for each compound (Table 3).

To better characterize the peptide spatial orientations, we plotted Edmundson wheel representations of peptides **1–6** (Fig. 2). The representation obtained for peptide **1** displays two clearly differentiated faces: the "charged face" (denoted in dashed blue line in Fig. 2) and a more extended "non-charged face" (denoted in full green line). The first face identifies residues R11, K4, K5 and R1 as those accounting for the mutual coulombic binding. The first three residues are located on the same side of the helical peptide and hence we designated it as the "charged face". These positively charged residues are able to produce salt bridges with the hydrophilic part of the lipids. The non-charged face is more extensive and is formed by six hydrophobic (M12, I5, W6, I3, W14 and F7) and two polar residues (N9 and Q2). However, it should be noted that **1** displays a homogeneously distributed remainder of the positively charged residues. Thus, residues K16, K13 and K10 are strategically intercalated along the "non-charged face". This is a striking difference with respect to peptide **2**, which displays two "charged faces" where all the cationic residues are concentrated. In peptide **2** there are two non-charged faces; however, it should be noted that even adding the two non-charged faces of peptide **2**, this portion is markedly lower with respect to the only non-charged face obtained for **1**. The Edmundson wheel representations obtained for peptides **3** and **4** are very similar displaying a very extensive charged face and a markedly reduced non-charged face. Peptide **5** in turn gives only a minimal non-charged zone corresponding to the W6 residue and the rest is "charged face". Obviously, peptide **6** displays a completely charged face because only cationic residues form it. Previously Lensink et al. [33] reported that a homogeneous distribution of positively charged residues along the axis of the helical peptide, and especially K4, R5, and K11 contribute to the association of peptide **1** with lipids. Our EDMC results are in a complete agreement with those MD simulations. In addition a very good correlation between the antifungal activities and the potential penetrating properties of these peptides are particularly striking.

2.2.2. SA results

The initial structure of peptides **1–6** was extended. The secondary structures of the lowest energy conformers calculated by DSSP program [34] are summarized in Table 4. The best structure of peptide **1** contains bends (I^3–W^6), 3_{10}-helix (F^7–N^9) and β-turn (R^{10}–R^{11}, K^{13}–K^{15}) and bends (F^7–N^9, R^{11}–K^{13}) in AMBER99 and OPLS-AA force field calculations, respectively. Hierarchical clustering shows bending and helical backbone structures for peptide **1** for the most representative clusters. OPLS-AA calculations, as in peptides **2–6**, predict H-bonds in other positions than AMBER99. Four H-bonds were formed between O(i) and H–N(j), two H-bonds between O(i) and H–N($i+3$), one H-bond between O(i) and H–N($i+2$), and O(i) and H–N($i+4$) (AMBER99 results). The results of OPLS-AA calculations predict eight H-bonds formed between O(i) and H–N(j), in peptide **1** four H-bonds between O(i) and H–N($i+2$) and two H-bonds between O(i) and H–N($i+4$), one between O(i) and H–N($i+3$). In peptide **2**, bend (Q^3–K^4, I6, Q^{12}–K^{13}) and

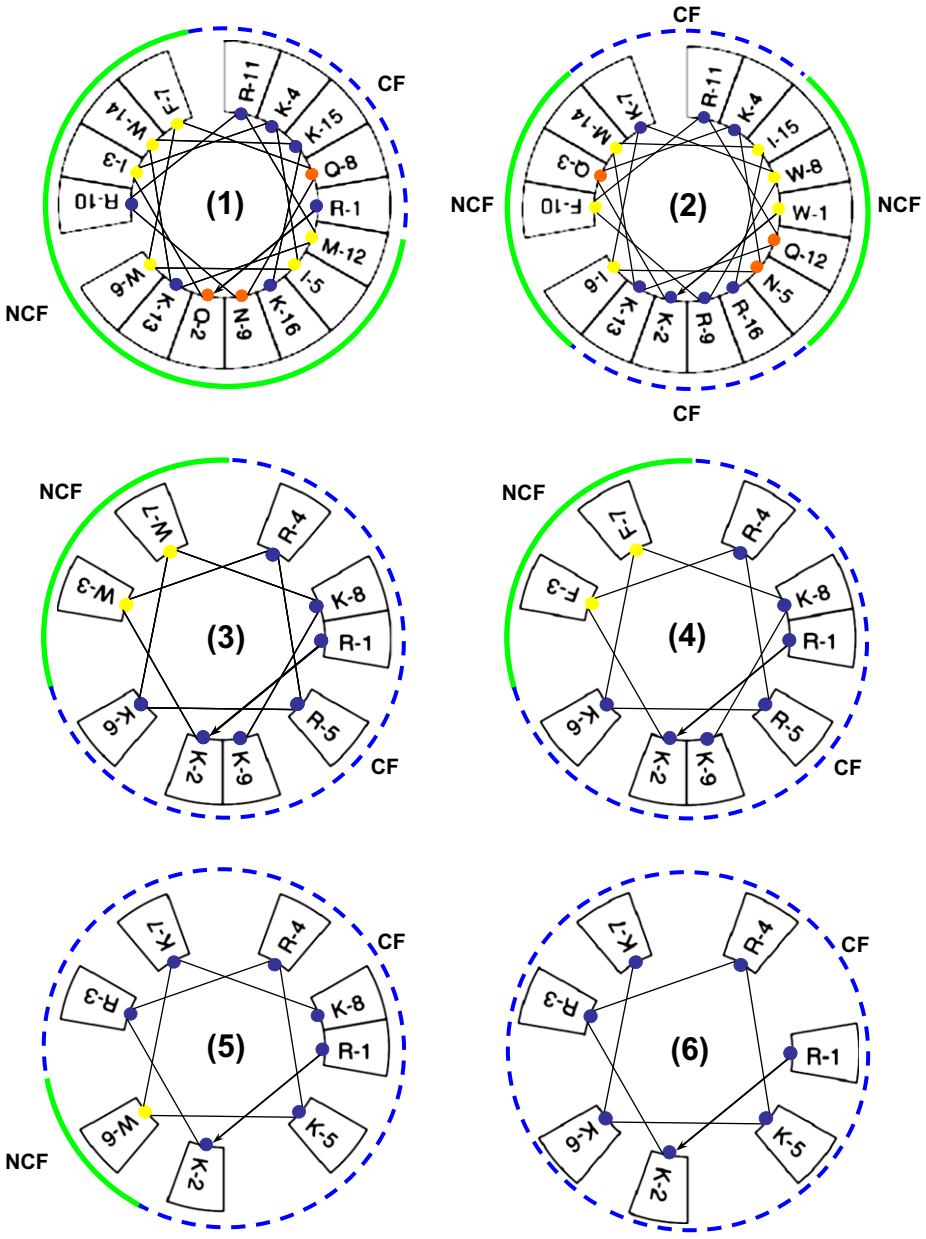

Fig. 2. Edmundson wheel representations of peptides **1**–**6**. The number in the center of the wheel corresponds to the peptide number. The ''charged'' (CF) and ''non-charged'' (NCF) faces are shown in blue dashed lines and full green lines, respectively. Positively charged amino acids are denoted with blue dots, the polar ones with orange, and the hydrophobic ones with yellow. (For interpretation of the references to colour in this figure legend, the reader is referred to the web version of this article.)

β-turn (W^8–F^{10}, M^{14}–I^{15}) alternate. Almost all of the bend structures remained (Q^3–N^5, F^{10}, K^{13}) and α-helix formed (I^6–R^9) which includes H-bonds. Peptides **3**–**6** contain α-helix, 3_{10}-helix and β-turn in the central residues in AMBER99 results. OPLS-AA predicts bend structures almost at the same residues.

2.2.3. MD simulations

In the trajectory analysis of peptides **1**–**6**, the total and potential energies, radius of gyration (R_g) and the RMSD of the backbone (N–C_α–$C_{(carbonyl)}$) atoms related to the structure at the end of equilibration (100 ps) were calculated (Figs. S1–S4 in Supplementary material). The root mean square fluctuation (RMSF) of the backbone atoms (Fig. S5 in Supplementary material) and the hydrophilic and hydrophobic solvent accessible surface areas (SASAs) were also calculated. The secondary structures of peptides were analyzed by sampling trajectories every 10 ps with the DSSP program [34].

In all peptides simulated here, the initial 3_{10}-helix was destroyed in the first 50–100 ps. The RMSD and the RMSF of the backbone during the simulation characterize this change in their secondary structure. The relative small change in the RMSD of the peptides in the trajectory is evidence for the stabilization of the backbone structure. RMSD for simulations

Table 4
Secondary structures of the best conformation of peptides **1**–**8** obtained from simulated annealing calculations by using AMBER99 and OPLS-AA force fields (FFs)

Peptide[a]	FF	Secondary structure[b]															
		Residue number															
		1	2	3	4	5	6	7	8	9	10	11	12	13	14	15	16
1	AMBER99	_	_	S	S	S	S	G	G	G	T	T	_	T	T	T	_
	OPLS-AA	_	_	_	_	_	_	S	S	S	_	S	S	S	_	_	_
2	AMBER99	_	_	S	S	_	S	_	T	T	T	_	S	S	T	T	_
	OPLS-AA	_	_	S	S	S	H	H	H	H	S	_	_	S	_	_	_
3	AMBER99	_	_	G	G	G	T	T	T	_							
	OPLS-AA	_	_	_	S	S	S	_	_	_							
4	AMBER99	_	_	T	T	T	T	T	_	_							
	OPLS-AA	_	_	_	S	S	S	S	_	_							
5	AMBER99	_	_	_	H	H	H	H	_								
	OPLS-AA	_	_	_	S	S	_	_	_								
6	AMBER99	_	_	G	G	G	_	_									
	OPLS-AA	_	_	S	S	S	S	_									
7	AMBER99	_	T	T	_												
	OPLS-AA	_	_	_	_												
8	AMBER99	_	T	T	_												
	OPLS-AA	_	_	_	_												

[a] Peptide codes used in Table 1.
[b] The secondary structure code obtained from DSSP program. H: 4-helix (α-helix); S: bend; G: 3-helix (3_{10}-helix); T: H-bonded turns; _: loops or irregular elements.

1–**6** is shown in Fig. S4 in Supplementary material. RMSD increased to 0.2–0.8 nm in all cases and remained almost constant in simulations **3**–**6**. The fluctuation in RMSD is attributed to slight changes in structure. In simulations **1** and **2** the conformations fluctuated between helical and turn/bend structures (Figs. 3 and 4).

The N- and C-terminal residues in all simulations appear to have a large flexibility as indicated by the change of RMSF values during the simulations. The change at central residues is moderate in simulations **1** and **2** (about 0.25 nm). The simulations **3**–**5** have shown a 0.15–0.20 nm change at residues 2–4 and 7. Also, the simulations **3** and **5** in the region which seems to be the most sensitive in the conformational change have a ~0.35 nm change at residues 5 and 4, respectively.

In all simulations, R_gs remained almost constant, except in 1 and 2, where the values fluctuated, but the secondary structures might be considered stable (Fig. S3).

The conformational changes in simulation **1** are shown in Fig. 3. The initial conformation returned and remained stable in simulation **1**, suggesting that the starting helical structure was destroyed to form a mixture of α-helix, β-turn and bend in the structure at residues 2–15. Such a conformational behavior was observed until the end of the simulation. The residues 4–6 have shown the highest preference for α-helix conformation. The initial and final residues appear to have a random coil structure because of the flexibility of these residues. For the same peptide in water Czajlik et al. [35] found a significant amount of helix-like conformation, even in a membrane-mimetic solvent system (TFE_{d2}/water = 9:1), by ^{1}H NMR. Thus, our MD simulation is in very good agreement with the experimental results. In simulation **2** (Fig. 4), the initial conformation of 3_{10}-helix was destroyed and α-helix, β-turn/bend and a stable random meander structures at the N- and C-terminal regions fluctuated during the whole simulation. The residues 5–10 have shown the highest preference of 3_{10}-helix conformation. Here, in peptide **2**, the β-turn and bend conformations were mainly formed at residues 2–4 and 11–15. Also in this simulation the initial and final residues appear to have random coil structure because of the flexibility of these residues. A mixture of coil, bend and *β*-turn conformations was formed after 86 ns of simulation. This mixture was observed until the end of the simulation. This is a different result with respect to the simulation performed on peptide **1**.

In simulations **3**–**6**, all derivatives adopt a helix-like conformation. However, while peptide **4** displays both α-helical and 3_{10}-helical features, the structure of peptide **3** is predominantly a 3_{10}-helix.

It is interesting to note that the vectors of the dipole moment of the solvent molecules had no definite direction in the periodic box. This indicates that the solvent had no electrostatic directional effect on the peptide structure. The largest deviation of the dipole moment at the wall of the periodic box was ±0.05 D.

In summary our MD simulations indicate that peptides **1**–**6** adopt a helix-like conformation. However, whereas peptide **1** displays a marked preference for an α-helix structure, peptide **2** shows a mixture of beta turn, bend and 3_{10}-helix, being the preferred form the 3_{10}-helix features.

2.3. Comparison of theoretical results obtained from different approaches

The energetically preferred cluster obtained with EDMC calculations for peptide **1** (70.48% of the total population) contains an α-helix structure, the second most populated cluster (7.46% of the total population) displays α-helix and β-turn structures. On the other hand, the energetically most stable form obtained in SA with minimization showed bend, 3_{10}-helix and β-turn structures using AMBER99 force field, and only bend and coil features using OPLS-AA force fields (see Table 4). The energetically preferred form of peptide **2** showed bend and β-turn structures for AMBER99 force field, and bend and α-helix structures for OPLS-AA force field. Peptides **3**–**6** showed structures with helical or consecutive turn secondary structures (AMBER99 force field) and bend with coil features (OPLS-AA force field). These peptides have shown a higher flexibility than peptides **1**–**2** due to their smaller size. In summary, AMBER99 force field has shown a slight preference for helical structures. Thus, this force field has a better correlation with ECCEP/3 force field than OPLS-AA force field. The OPLS-AA results differ significantly showing some differences in φ and ψ angle values and H-bond positions. Despite this fact, all force fields used here predict a helix-like structure for peptides **1**–**6**. The N- and C-terminal residues have shown a high flexibility, since no regular stable structure could be observed.

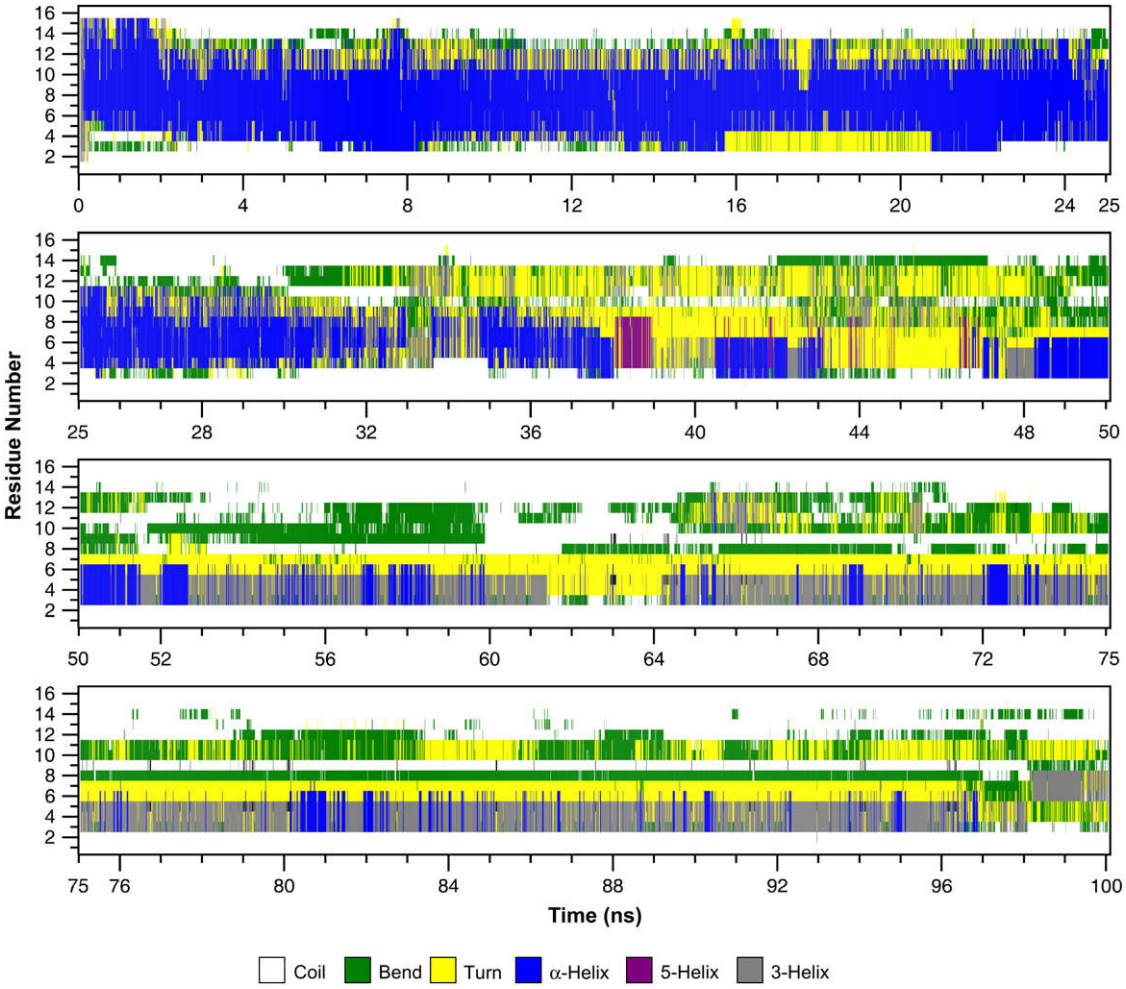

Fig. 3. Change in the secondary structure during molecular dynamics simulation for peptide **1**.

These results support the use of the MD simulations for these peptides. It is clear, however, that in order to obtain a relatively complete picture about the conformational intricacies of peptide **1** and derivatives at least 100 ns of simulation appears to be necessary. Such simulations can provide useful information about the conformational preferences and molecular flexibility of **1** and derivatives, which might be useful to get a more profound understanding of the biological response of these peptides.

Comparing the results obtained for the conformational analysis using the different approaches, we can conclude that, in general, these methods predict a helix-like structure for peptide **1** and derivatives. These results are also in agreement with the experimental results obtained from NMR [35].

2.4. Molecular electrostatic potentials (MEPs)

Knowledge of the stereoelectronic attributes and properties of peptide **1** and derivatives will contribute significantly to the elucidation of the molecular mechanism involved in the antifungal activity. Molecular electrostatic fields and molecular electrostatic potentials (MEPs), which are their visualisation, offer an informative description of the capacity of peptides to generate stereoelectrostatic forces. Thus, the electronic study of peptides was performed using MEPs [36]. MEPs have been shown to provide reliable information, both on the interaction sites of molecules with point charges and on the comparative reactivities of those sites [36,37]. More positive potentials reflect nucleus predominance, while less positive values represent rearrangements of electronic charges and lone pairs of electrons. The fundamental application of this study is the analysis of non-covalent interactions [37], mainly by investigating the electronic distribution in the molecule. Thus, this methodology was used to evaluate the electronic distribution around molecular surface for peptides reported here. The MEPs of peptide **1** are shown in Fig. 5 and the MEPs of peptides **3** and **6** are plotted in Fig. 6. We evaluated the MEPs of all peptides tested but we show here only the MEPs obtained for the three peptides, which displayed a significant antifungal activity.

To better appreciate the electronic behavior of **1** and considering that two different faces were signalled in Fig. 2, we present the MEPs of **1**, showing the two faces of this peptide (Fig. 5). Fig. 5a gives the ‘‘charged face’’ (CF) characterized by the presence of four cationic residues (R1, K4, R11 and K15). Although it is possible to visualise residue K16 near

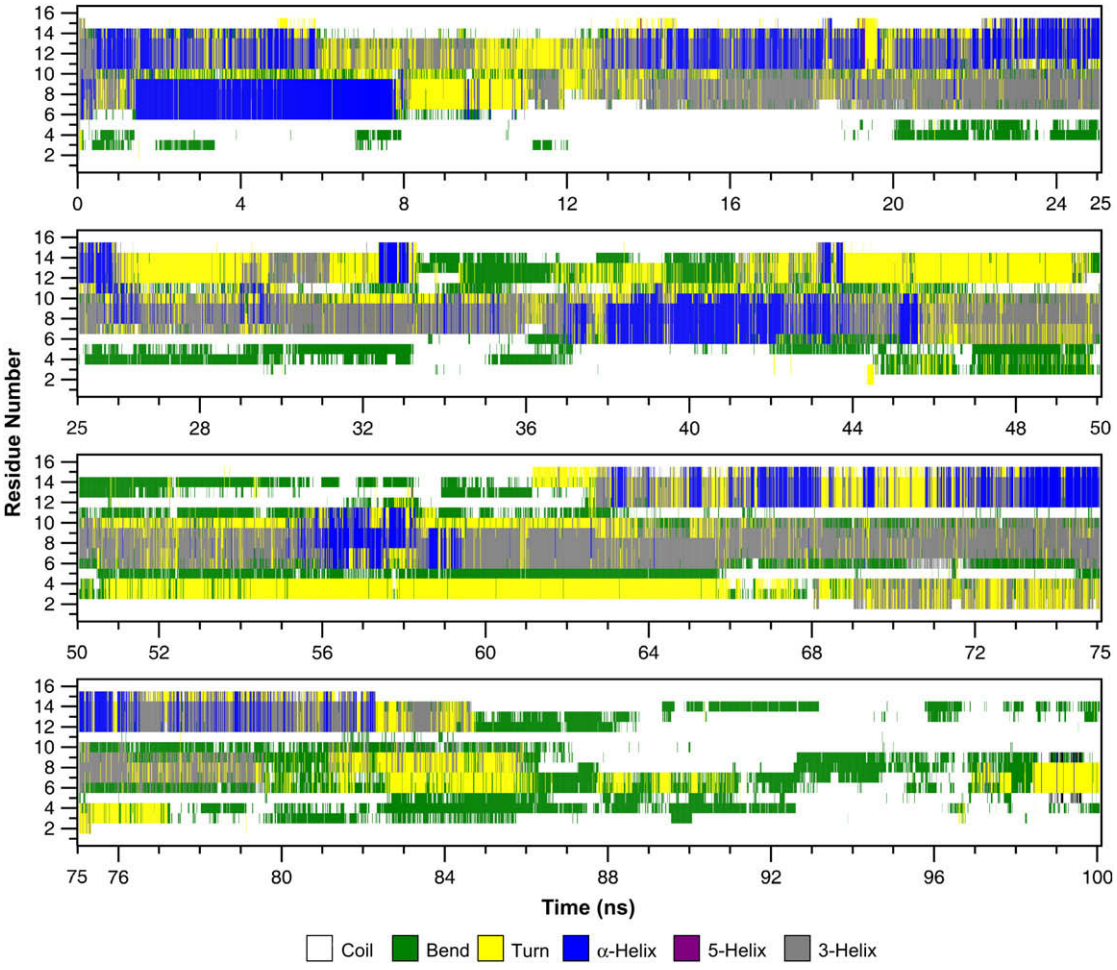

Fig. 4. Change in the secondary structure during molecular dynamics simulation for peptide **2**.

to this face, in fact this residue is somewhat shifted in the direction of the non-charged face. It has been previously reported that peptide–lipid association occurs through formation of salt bridges between the positively charged residues K4, R11 and K15 and the lipid phosphate groups [33]. In addition, tryptophan fluorescence studies previously showed the importance of peptide with positively charged residues for the initial binding to negatively charged vesicles, since double R/K → A mutations involving the residues K4/R10/R11/K13/K15 significantly decreased the binding affinity [38]. The MEPs of **1** suggest that the above-mentioned residues (R1, K4, R11 and K15) could be responsible for the initial binding. The previously reported [33] π-stacking interaction between F7 and R11 residues might be also appreciated on this face. Although the main positive potentials ($V(r)$ ranging from 0.60 to 0.43 el au^{-3}) are concentrated on this face, it should be noted that there is a relatively homogeneous distribution of positively charged residues along the entire structure. Thus, residues R10, K16 and K13 are strategically located in an alternated fashion within the non-charged face.

Since the non-charged moiety is too large, two different views of the MEPs were plotted in order to better visualise this face (Fig. 5b and c). Fig. 5b displays four hydrophobic residues I3, W6, F7 and W14. It appears that a kind of π-stacking cluster through W6/R10/W14 occurs in this portion of **1**. Lensink et al. [33] reported that these residues could protect the peptide from the water phase. A clear hydrophobic interaction between I3 and W6 might be also appreciated in this figure. Fig. 5c displays a more polar face in comparison to Fig. 5b, since it possesses the three polar residues of **1** (Q2, Q8 and N9). Interestingly, I5 is located in an intercalated position with respect to polar residues and therefore there are no interactions between them. These results suggest that these polar residues could be highly solvated. Mutation of either tryptophan decreases internalization, whereas double substitution completely inhibits peptide internalization [19,22,39]. These results indicate that peptide **1** is not sufficiently hydrophobic to insert deeply into phospholipid model membranes [21,40]. Therefore charge neutralization is required for a deeper insertion of the peptide into the hydrophobic core of the membrane. The extended non-charged face alternating cationic residues among the hydrophobic and polar ones observed in the MEPs of **1** appears to be operational in this sense.

Fig. 6a gives the MEPs obtained for peptide **3**. This surface shows a more extended positively charged face with respect to

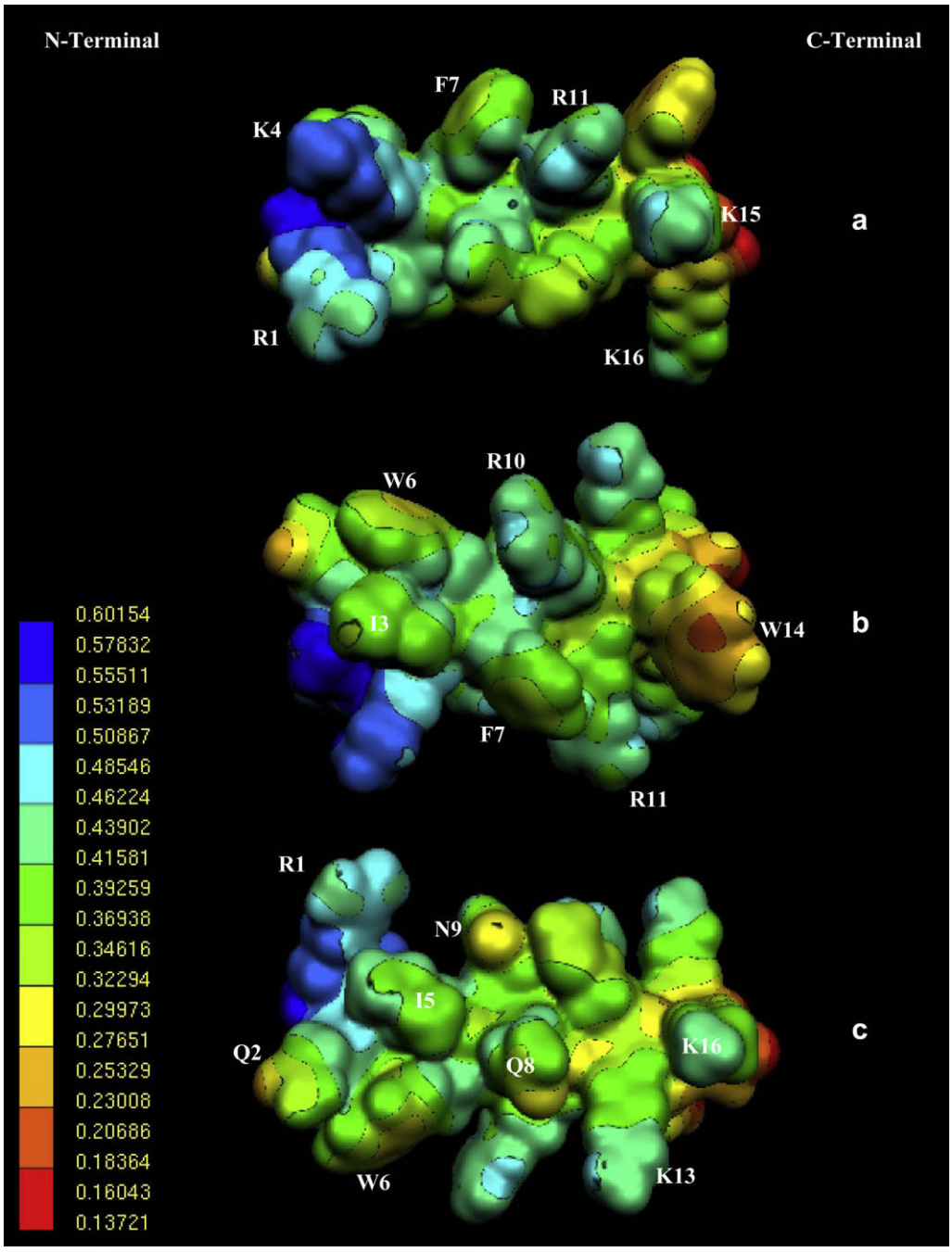

Fig. 5. Electrostatic potential-encoded electron density surfaces of peptide **1**. (a) "Charged face", (b) and (c) two different views of the "non-charged face". The surfaces were generated with Gaussian 03 using RHF/6-31G single point calculations. The coloring represents electrostatic potential with red indicating the strongest attraction to a positive point charge and blue indicating the strongest repulsion. The electrostatic potential is the energy of interaction of the positive point charge with the nuclei and electrons of a molecule. It provides a representative measure of overall molecular charge distribution. The colour-coded is shown at the left. (For interpretation of the references to colour in this figure legend, the reader is referred to the web version of this article.)

1. In this portion are located five cationic residues R4, K8, R1, R5 and K9. The MEPs obtained for peptide **6** are shown in Fig. 6b. A very extensive deep blue zone with potential values in the order of 0.60 el au^{-3} clearly dominates this surface.

Previously reported MD simulations indicated that the aromatic residues do not contribute to the initial binding, but rather to the subsequent insertion of peptide **1** between the bilayer head groups, where they shield the peptide from the aqueous phase [33]. The importance of hydrophobic residues seems to be crucial for the antifungal activity as well. Comparing the MEPs obtained for peptides **1**, **3** and **6** it is evident that they correlate very well with their antifungal activities: the most active peptide of this series, intermediate activity and completely inactive molecule, respectively. These results lend additional support for the key role of the hydrophobic residues in these peptides acting as antifungal compounds.

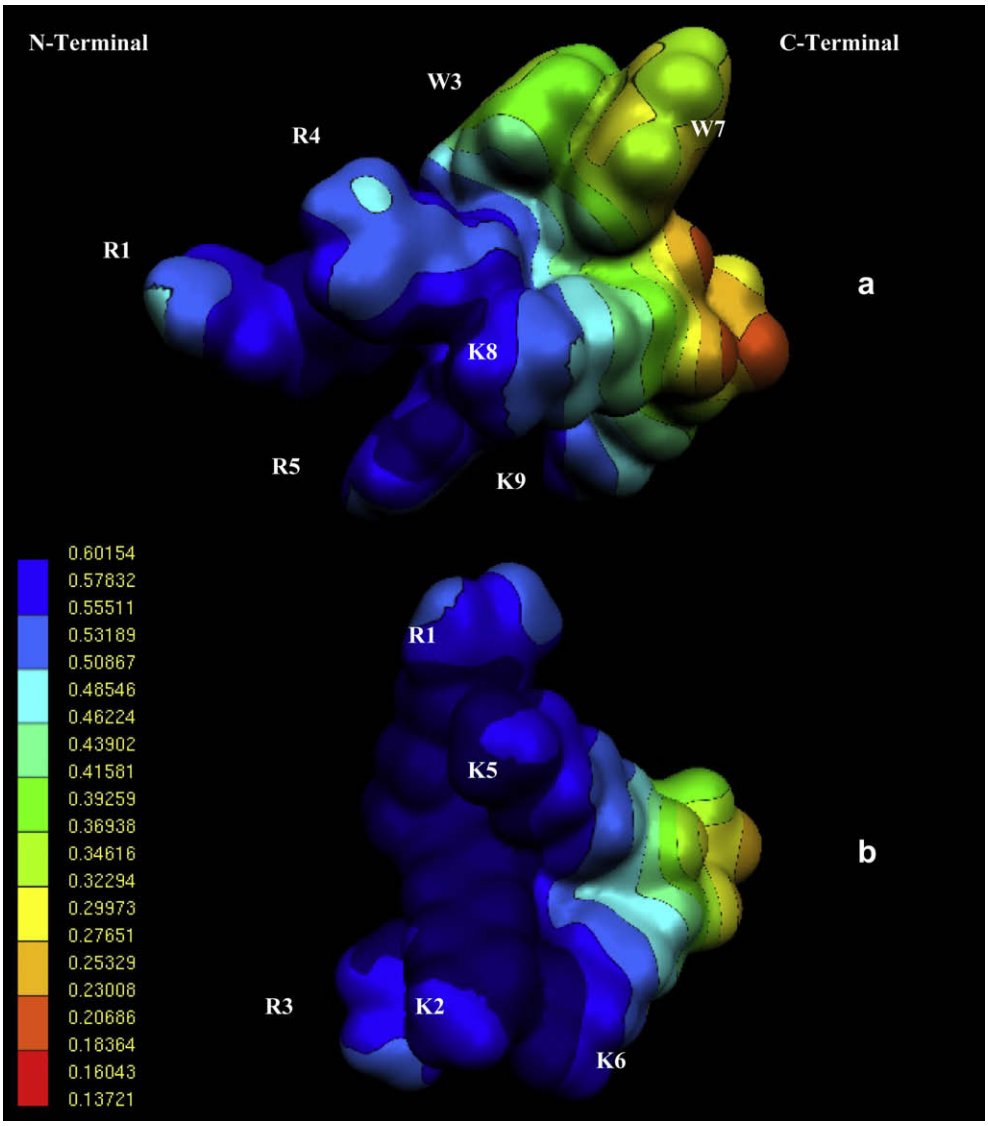

Fig. 6. Electrostatic potential-encoded electron density surfaces of peptides **3** (a) and **6** (b). The colour-coded is shown at the left. (For interpretation of the references to colour in this figure legend, the reader is referred to the web version of this article.)

2.5. Small size antifungal peptides

The consideration, that a peptide-based antifungal agent should be as short as possible in order to reduce costs, prompted us to synthesize even shorter derivatives of **1**. Thus, with the aim to predict the potential antifungal effect of small size peptides, we performed a molecular modeling study in a series of tetrapeptides. Several different tetrapeptides were modeled; however, we report here only the results obtained for two of them (KWKK–NH_2 (**7**) and RQKK–NH_2 (**8**)), being representative of the entire series.

Tetrapeptides **7** and **8** displayed a completely different conformational and electronic behavior. EDMC, SA and MD results obtained for these peptides are summarized in Tables 3 and 4 and Tables SVII–SVIII and Figs. S1–S5 in Supplementary material, respectively. EDMC results obtained for tetrapeptides **7** and **8** predict a higher molecular flexibility in comparison to the longer peptides. Also, considering the length of the backbone of these peptides they cannot achieve a stable structure. Although both tetrapeptides display a statistical coil [41] structure, their conformational preferences are markedly different. Whereas peptide **7** displays a quasi-π-helix form ($\psi_1 = -62.9$, $\phi_2 = -88.1$, $\psi_2 = 81.8$, $\phi_3 = -86.4$, $\psi_3 = 72.3$ and $\phi_4 = -82.7$), peptide **8** prefers a quasi-α-helix structure ($\psi_1 = -18.7$, $\phi_2 = -73.9$, $\psi_2 = -25.5$, $\phi_3 = -82.3$, $\psi_3 = -27.6$ and $\phi_4 = -78.4$). This is a striking difference obtained for these tetrapeptides. SA calculations indicate that these peptides are more flexible than peptides **1**–**6** (Table 4). The small size of these peptides could explain the irregular structures obtained for peptides **7**–**8** (OPLS-AA force field), whereas turn structures were preferred for the central residues of these peptides (AMBER99). MD calculations indicate that peptides **7** and **8** show a statistical coil structure during the whole simulation time because of their high flexibility. However, from MD a clear difference obtained for these tetrapeptides is that peptide **8** displays a tendency to adopt a turn

conformation, whereas peptide **7** has the tendency to achieve extended conformations. The spatial ordering adopted by peptide **8** is closely related to that obtained for the first four residues of peptide **1** (see Fig. 7c right hand).

Fig. 7 gives the MEPs obtained for compounds **1**, **3** and **8** in a front view. The similar MEP values obtained for peptides **1** and **8** can be appreciated in this figure. In contrast a more positively charged MEP was obtained for compound **3** as it was previously discussed.

On the basis of the stereoelectronic similarity obtained for peptides **1** and **8**, it is reasonable to think that tetrapeptide **8** could present some antifungal activity, but not peptide **7**. Thus, to confirm our hypothesis, we decided to test the antifungal effects of tetrapeptides **7** and **8**. As expected, peptide **7** did not show any antifungal activity with the concentrations reported here. In contrast, peptide **8** displayed a moderate but significant antifungal effect against *C. neoformans* (Table 1). It must be pointed out that peptide **8** displays antifungal activity

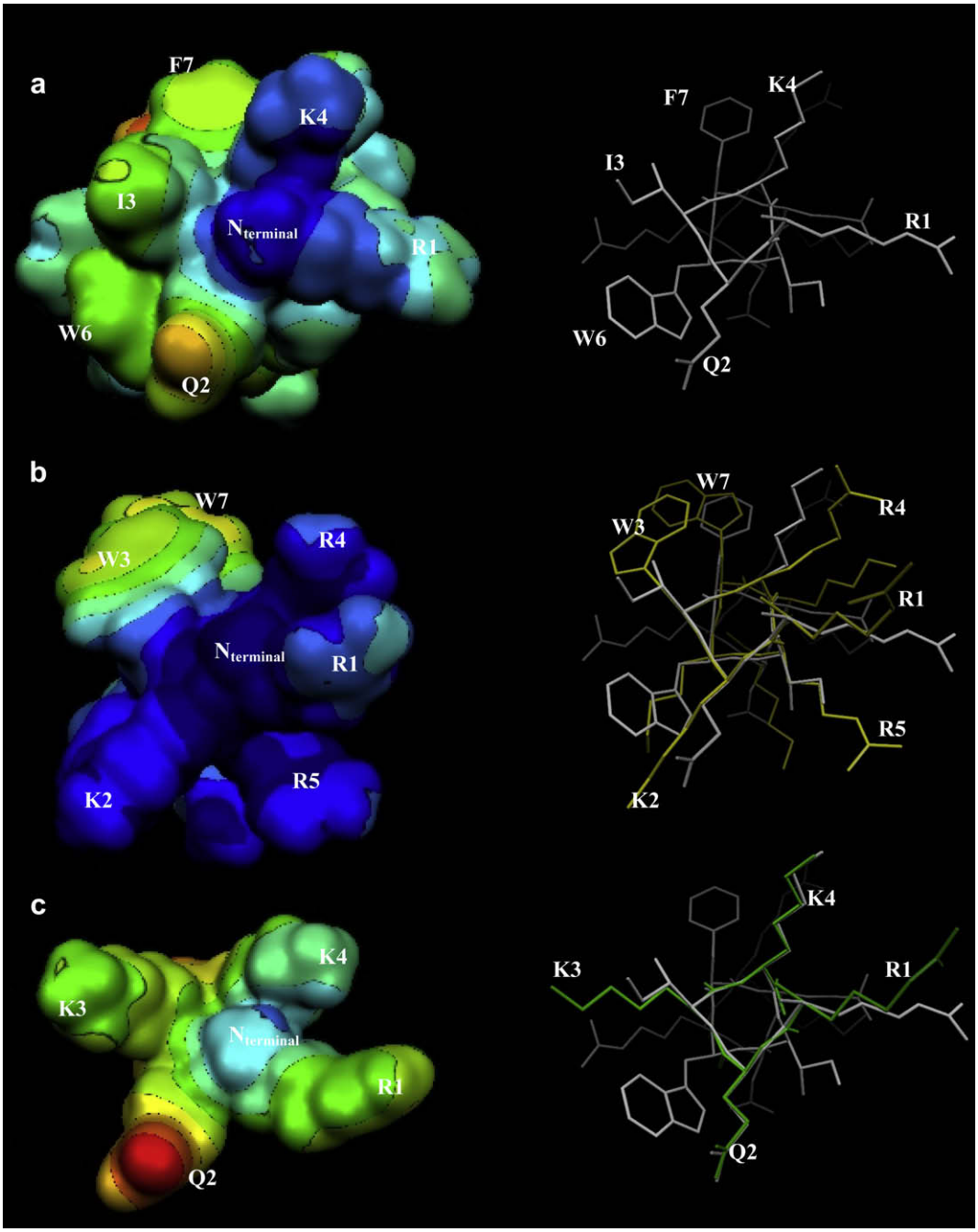

Fig. 7. Electrostatic potential-encoded electron density surfaces obtained for peptides **1** (a), **3** (b) and **8** (c) in a front view of the N-terminal portion (left hand). Also this figure shows at the right hand: (a) a frontal spatial view of **1**, (b) an overlapped stereoview of peptide **1** (white) with peptide **3** (yellow), and (c) an overlapped stereoview of peptide **1** (white) with peptide **8** (green). (For interpretation of the references to colour in this figure legend, the reader is referred to the web version of this article.)

only against *C. neoformans*; in contrast this compound was not active against *C. albicans*. This is a striking difference with respect to **1**. It is clear, however, that the antifungal potency found for **8** against *C. neoformans* is very interesting particularly considering its small size.

Inspection of Fig. 7 led us to appreciate that although peptides **1**, **3** and **8** are of different size, they display some stereoelectronic similarities primarily near the N-terminal portion, implicating a likely overlap on these moieties. Cellular uptake experiments previously demonstrated the crucial role of arginines in cell-penetrating peptides [42]. Also, MD simulations indicated that arginine residues could be responsible for the initial electrostatic binding forming bidentate hydrogen bonds with lipid phosphate groups. It should be noted that the first residue of peptides **1**, **3** and **8** is arginine. In fact there are various ways in which **8** may produce its antifungal activity, on which we can only speculate. In that respect the similar stereoelectronic behaviors observed between **8** and the N-terminal portions of **1** and **3** are particularly noteworthy.

3. Conclusions

In the present paper, we report the design, synthesis and antifungal effects of peptide **1** and derivatives, a new series of antifungal peptides. Among the peptides tested, RQIKIWFQNRRMKWKK–NH_2 (**1**), RKWRRKWKK–NH_2 (**3**) and RQKK–NH_2 (**8**) displayed the most powerful inhibitory effect against *C. neoformans*. A detailed conformational and electronic study supported by theoretical calculations helped us to identify a possible "biologically relevant conformation" for these peptides. A particular combination of cationic and hydrophobic residues adopting a definite spatial ordering appears to be the key parameter for the transition from hydrophilic to hydrophobic phase, which could be a necessary step to produce the antifungal activity. We believe that our results could contribute to an understanding of the minimal structural requirements for the antifungal potential of peptides reported here and to the design of novel structurally related agents. These results are very encouraging in that they show a great potential for peptides **1** and **8** as a truly novel class of antifungal compounds particularly against the yeast *C. neoformans*. Thus, the antifungal activity reported in this paper for peptides **1** and **8** opens promising ways for the development of a new antifungal agent for treatment of cryptococcosis. Since *C. neoformans* remains an important life-threatening complication for immunocompromised hosts, particularly for patients who have undergone transplantation of solid organs and therefore, new compounds effectively acting against this fungus are highly needed [43,44].

Peptide **1** has been used as a non-viral, non-toxic and highly efficient vector for delivering bioactive substances, that by themselves are membrane-impermeable, to the cytoplasm or nucleus of cells [18,19]. The antifungal activity found for **1** is very interesting by itself but it is also important considering its potential use as a carrier for other known antifungal drugs. Thus, this system may improve the pharmaceutical properties of the drugs by, for example, improving solubility and bioavailability, or by minimizing toxicity and overcoming drug resistance.

4. Experimental section

4.1. Synthetic methods

Solid phase synthesis of **1**, RQIKIWFQNRRMKWKK–NH_2, was carried out manually on a *p*-methylbenzhydrylamine resin (MBHA, 0.39 mmol/g) with standard methodology using Boc-strategy. Side chain protecting groups were as follows: Tos for Arg and 2-chloro-Z for Lys. All protected amino acids were coupled in CH_2Cl_2 or CH_2Cl_2/DMF solvent mixture in a ratio of 1:1 (for Gln and Asn) using DCC (2.5 equiv.) and HOBt (2.5 equiv.). Amino acid incorporation was monitored by Kaiser [45] ninhydrin test. After coupling of the amino acid, Boc-deprotection was effected by using TFA/CH_2Cl_2 (1:1) for 5 min first then repeated for 25 min. The completed peptide resin was treated with liquid HF/dimethyl sulfide/anisole/indole (86:6:4:2) at 5 °C for 1 h. HF was removed and the resulted free peptide was solubilized in 10% aqueous acetic acid and lyophilized. The crude peptide was purified by semi-preparative RP HPLC on a Lichrosorb C-18 column (16 × 250 mm, 7 μm) with a linear gradient of acetonitrile 30–100%, 0.1% TFA in 70 min, 4 ml/min flow. The appropriate fractions were pooled and lyophilized. The purified peptide was characterized by HPLC and mass spectrometry using a Finnigan TSQ 7000 tandem quadrupole electrospray mass spectrometer. M + H calc.: 2244.3, found: 2244.5. Analytical HPLC conditions: column: Luna C-18, 5 μm, 4.6 × 250 mm; gradient: 30–50% AcN, 0.1% TFA in 10 min, 1.2 ml/min flow, 220 nm. R_t: 4.280 min. Same synthesis procedures and analytical HPLC conditions were applied for the peptide analogues (**2**–**8**) as follows:

	Retention factor (min)	Gradient elution (%)
RQIKIWFQNRRMKWKK–NH_2 (**1**)	4.280	30–50 (10 min)
WKQKNIKWRFRQKMIR–NH_2 (**2**)	11.200	5–80 (25 min)
RKWRRKWKK–NH_2 (**3**)	13.200	5–35 (15 min)
RKFRRKFKK–NH_2 (**4**)	9.387	5–30 (10 min)
RKRRKWKK–NH_2 (**5**)	9.339	5–35 (15 min)
RKRRKKK–NH_2 (**6**)	4.576	5–35 (15 min)
KWKK–NH_2 (**7**)	9.012	5–35 (15 min)
RQKK–NH_2 (**8**)	3.553	5–20 (15 min)

Mass spectrometric analysis of peptides **1**–**8** is given in Supplementary material.

4.2. Antifungal evaluation

4.2.1. Microorganisms and media

For the antifungal evaluation, standardized strains from the American Type Culture Collection (ATCC), Rockville, MD, USA, were used (*C. albicans* ATCC 10231 and *C. neoformans* ATCC 32264). Active compounds were tested against clinical isolates from the Malbrán Institute [(M), Av. Velez Sarsfield 563, Buenos Aires]. The isolates included 10 strains of *C. neoformans* which *voucher specimens* are presented in Table 2.

Strains were grown on Sabouraud–chloramphenicol agar slants for 48 h at 30 °C, maintained on slopes of Sabouraud–dextrose agar (SDA, Oxoid) and sub-cultured every 15 days to prevent pleomorphic transformations. Inocula of cells were obtained according to reported procedures and adjusted to $1-5 \times 10^3$ cells with colony forming units (CFU)/ml [46].

4.3. Antifungal susceptibility testing

4.3.1. MIC determinations

MIC of each extract or compound was determined by using broth microdilution techniques according to the guidelines of the Clinical and Laboratory Standards Institute (CLSI), formerly National Committee for Clinical and Laboratory Standards for yeasts (M27-A2) [46]. MIC values were determined in RPMI-1640 (Sigma, St. Louis, MO, USA) buffered to pH 7.0 with MOPS. Microtiter trays were incubated at 35 °C in a moist, dark chamber, and MICs were visually recorded at 48 h. For the assay, stock solutions of pure compounds were twofold diluted with RPMI from 256 to 0.98 μg/ml (final volume = 100 μl) and a final DMSO concentration ≤1%. A volume of 100 μl of inoculum suspension was added to each well with the exception of the sterility control where sterile water was added to the well instead. Ketoconazole, amphotericin B and itraconazole (all from Sigma Chemical Co., St. Louis, MO, USA) were used as positive controls. Endpoints were defined as the lowest concentration of drug resulting in total inhibition (MIC_{100}) of visual growth compared to the growth in the control wells containing no antifungal. MIC_{80} and MIC_{50} were defined as the lowest concentration of a compound that caused 80 and 50% reduction of the growth control, respectively (culture media with the microorganism but without the addition of any compound) and were determined spectrophotometrically with the aid of a VERSA Max microplate reader (Molecular Devices, USA). The MFC of peptide **1** against each isolate was also determined as follows: after determining the MIC, an aliquot of 5 μl sample was withdrawn from each clear well of the microtiter tray and plated onto a 150 mm RPMI-1640 agar plate buffered with MOPS (Remel, Lenexa, KS). Inoculated plates were incubated at 30 °C and MFC was recorded after 48 h. The MFC was defined as the lowest concentration of each compound that resulted in total inhibition of visible growth. All tests were performed in duplicates.

4.3.2. Determination of percentage of inhibition

The test was performed in 96-well microplates. Peptide test wells (PTWs) were prepared with stock solutions of each peptide in DMSO (maximum concentration ≤ 2%), diluted with RPMI-1640 to final concentrations 200–12.5 μM. Inoculum suspension (100 μl) was added to each well (final volume in the well = 200 μl). A growth control well (GCW) (containing medium, inoculum, the same amount of DMSO used in PTW, but compound-free) and a sterility control well (SCW) (sample, medium and sterile water instead of inoculum) were included for each strain tested. Microtiter trays were incubated in a moist, dark chamber at 35 °C, 24 or 48 h for *Candida* spp. or *Cryptococcus* sp., respectively. Microplates were read in a VERSA Max microplate reader (Molecular Devices, Sunnyvale, CA, USA). Amphotericin B was used as positive control (100% inhibition). Tests were performed in duplicates. Reduction of growth for each peptide concentration was calculated as follows: % of inhibition = $100 - (OD_{405}$ PTW − OD_{405} SCW)/OD_{405} GCW − OD_{405} SCW.

Statistical analysis: Data were statistical analyzed by one-way analysis of variance. A p value of <0.05 was considered significant.

4.4. Computational methods

4.4.1. EDMC calculations

The conformational space of each peptide was explored using the method previously employed by Liwo et al. [47] that included the electrostatically driven Monte Carlo (EDMC) method [29]. Conformational energy was evaluated using the ECEPP/3 force field [48]. This force field employs rigid valence geometry. Hydration energy was evaluated using a hydration-shell model with a solvent sphere radius of 1.4 Å and atomic hydration parameters that have been optimized using nonpeptide data (SRFOPT) [49]. In this model, in addition to a sum of electrostatic, non-bonding, hydrogen bond and torsional energy terms, the total conformational energy includes terms accounting for loop closing and peptide solvation. The conformation with minimized energy was subsequently perturbed by changing its torsional ϕ and Ψ angles using the Monte Carlo method [50]. Piela's algorithm [51], which was also applied at this stage, greatly improves the acceptance coefficient. In this algorithm ϕ and Ψ angles are changed in a manner which allow the corresponding peptide group to find the most proper orientation in the electrostatic field of the rest of the peptide chain. The energy of the new conformation is minimized, compared to the previous one and may be accepted or discarded on the basis of energy and/or geometry. If the new energy-minimized conformation is similar in shape and in energy to the starting conformation, it is discarded. Otherwise, the energy of the new conformation is compared to the energy of the parent conformation. If the new energy is lower, the new conformation is accepted unconditionally, otherwise the Metropolis criterion [52] is applied in order to accept or reject the new conformation. If the new conformation is accepted, it replaces the starting one; otherwise another perturbation of the parent conformation is tried. A temperature jump may be included if the perturbation is not successful for an arbitrarily chosen number of iterations. The process is iterated until a sufficient number of conformations have been accepted. The detailed procedure is described in Ref. [53].

In order to explore the conformational space extensively, we carried out 10 different runs, each of them with a different random number, for each peptide studied. Since the EDMC procedure uses random numbers, there is a need to initialize the random number generator by providing an integer. Therefore, we collected a total of 5000 accepted conformations for each peptide studied. Each EDMC run was terminated after 500 energy-minimized conformations had been accepted.

The parameters controlling the runs were the following: a temperature of 298.15 K was used for the simulations. A temperature jump of 50 000 K was used and the maximum number of allowed repetitions of the same minimum was 50. The maximum number of electrostatically predicted conformations per iteration was 400; the maximum number of random-generated conformations per iteration was 100; the fraction of random/electrostatically predicted conformations was 0.30. The maximum number of steps at one increased temperature was 20 and the maximum number of rejected conformations until a temperature jump executed was 100. Only *trans* peptide bonds ($\omega \cong 180°$) were considered.

The ensemble of obtained conformations was then clustered into families using the program ANALYZE [54], which applies the minimal-tree clustering algorithm for separation, using all heavy atoms, energy threshold of 30 kcal mol^{-1}, and RMSD of 0.75 Å as separation criteria for all peptides studied here. Molecules containing seven, eight and 16 amino acids residues were clustered using the same method but instead of using all heavy atoms it used only the backbone atoms (C_α, N and $C_{(carbonyl)}$). This procedure allows for substantial reduction of the number of conformations and eliminates repetitions.

4.4.2. SA calculations

To find the best structures of peptides studied, 5000 structures were generated by simulated annealing (SA) implemented in Tinker Version 4.2 [55]. Peptides were generated by the software and minimized with a charge and van der Waals cutoff of 1.8 and 1.4 nm, respectively, with OPLS-AA and AMBER99 force fields. A taper of 0.8 was applied to smooth the cutoff to zero in the calculations. The solvation was simulated by GB/SA (generalized Born/surface area) model. The tolerance of the minimization was 0.001 kcal mol^{-1} Å^{-1}. The following protocol was used in the simulated annealing: 5000 times were repeated 2000 steps equilibration in 1000 K and 2000 steps cooling to 50 K exponentially with 1 fs step-size. After cooling the structures were minimized with the previous method. The minimized structure was applied for the next step. The secondary structures of the peptides were analyzed by DSSP [34]. The algorithm measures the geometry and the hydrogen bonding in peptides. The secondary structures are assigned by the following way: turns within 3, 4 and 5 residues, respectively, are assigned on the basis of hydrogen bonds between i to $i+1$ (three residue turn), i to $i+1$ or $i+2$ (four residue turn), i to $i+1$ or $i+2$ or $i+3$ (five residue turn). A β-bridge is assigned when two non-overlapping stretches of three residues each, $i-1$, i, $i+1$ and $j-1$, j, $j+1$ form H-bonding parallel or antiparallel pattern. Two or more consecutive β-bridge structures are assigned as β-sheet structures. A bend is defined as a five residue turn without H-bonds with a curvature of at least 70° between the first three residues ($i-2$, $i-1$ and i) and the last three residues (i, $i+1$ and $i+2$). The position of the bend is marked at i. Two consecutive turns at position $i-1$ and i form a helix. 3_{10}-Helix is marked at positions i, $i+1$ and $i+2$. α-Helix and π-helix at i, $i+1$, $i+3$ and i, $i+1$, $i+2$, $i+3$, $i+4$, respectively. Residues without recognized secondary structures are assigned as irregular or loop (random coil) structure. For clustering 5000 structures a perl script in MMTSB [56] was used.

4.4.3. MD simulations

Molecular dynamics (MD) simulations were performed using the GROMACS 3.2.1 package of programs [31,32], with the OPLS-AA force field [57–59]. The calculations were carried out using a standard helix 3_{10} ($\phi = -49.00°$, $\psi = -26.00°$) as a starting structure. The peptides **1**–**8** were embedded in a box containing the SPC water model [60] that extended to at least 10 Å between the solutes and the edge of the box. The total number of water molecules was between 1389 and 2791. Then Cl^- ions were added to the systems by replacing water molecules in random positions, thus making the whole system neutral. For details see Table SIX in Supplementary material. Prior to dynamics simulation, internal constraints were relaxed by energy minimization. Following the minimization, an MD equilibration run was performed under position restraints for 20 ps. An unrestrained run was then initiated. During the MD runs, the LINCS algorithm [61] was used to constrain the lengths of hydrogen containing bonds; the waters were restrained using the SETTLE algorithm [62]. The time step for the simulations was 0.002 ps. The simulations were run under NPT conditions, using Berendsen's coupling algorithm [63] for keeping the temperature and pressure constant ($P = 1$ bar, $\tau_P = 0.5$ ps; $T = 310$ K, $\tau_T = 0.1$ ps). The compressibility was 4.8×10^{-5} bar^{-1}. Van der Waals forces were treated using a 12 Å cutoff. Long-range electrostatic forces were treated using the particle mesh Ewald method (PME) [64]. The coordinates were saved every 10 ps. The total simulation time was 100 ns for every peptide. The analysis of the simulations was performed using the analysis tools provided in the GROMACS package.

4.4.4. Molecular electrostatic potentials

Quantum mechanics calculations were carried out using the Gaussian 03 program [65]. We use the most populated conformations of peptides **1**–**8** obtained from EDMC calculations. Subsequently, single point *ab initio* (RHF/6-31G(d)) calculations were carried out. The electronic study was carried out using molecular electrostatic potentials (MEPs) [36]. These MEPs were calculated using RHF/6-31G(d) wave functions and MEP graphical presentations were created using the MOLEKEL program [66].

Acknowledgements

This work is part of the Hungarian-Argentine Intergovernmental S&T Cooperation Programme and was supported by the Research and Technological Innovation Foundation and by the SECyT, as well as by grants from Universidad Nacional de San Luis and grants to S.A.Z. and R.D.E. from the Agencia de Promoción Científica y Tecnológica de la Argentina (ANPCyT) PICT R 260. It is part of the Iberoamerican Program of Science and Technology for the Development (CYTED,

Network RIBIOFAR). T.K. and B.P. thank the Hungarian Research Fund OTKA K61577. R.D.E. is a member of the CONICET (Argentina) staff. M.F.M is a fellow of CONICET (Argentina). M.F.M. is a recipient of a Bernouilli Fellowship from the University of Groningen. The authors thank E. Menyhárt for the technical assistance of peptide synthesis.

Appendix. Supplementary material

Supplementary data associated with this article can be found in the online version, at doi:10.1016/j.ejmech.2008.02.019.

References

[1] T.J. Walsh, A. Groll, J. Hiemenz, R. Fleming, E. Roilides, E. Anaissie, Clin. Microbiol. Infect. 10 (2004) 48–66.
[2] N. Georgopapadakou, J. Tkacz, Trends Microbiol. 3 (1995) 98–104.
[3] M. Nagiec, E. Nagiec, J. Baltisberger, G. Wells, R. Lester, R. Dickson, J. Biol. Chem. 272 (1997) 9809–9817.
[4] S. Ablordeppey, P. Fan, I. Ablordeppey, L. Mardenborough, Curr. Med. Chem. 6 (1999) 1151–1195.
[5] T. White, K. Marr, R. Bowden, Clin. Microbiol. Rev. 11 (1998) 382–402.
[6] A. Polak, Mycoses 42 (1999) 355–370.
[7] J. Bartroli, E. Turmo, M. Algueró, E. Boncompte, M. Vericat, L. Conte, J. Ramis, M. Merlos, J. García-Rafanell, J. Forn, J. Med. Chem. 41 (1998) 1855–1868.
[8] J. Bartroli, E. Turmo, M. Algueró, E. Boncompte, M. Vericat, L. Conte, J. Ramis, M. Merlos, J. García-Rafanell, J. Med. Chem. 41 (1998) 1869–1882.
[9] R.E.W. Hancock, R. Leher, Trends Biotechnol. 16 (1998) 82–88.
[10] P. Bulet, R. Stöcklin, Protein Pept. Lett. 12 (2005) 3–11.
[11] M.F. Masman, A.M. Rodríguez, L. Svetaz, S.A. Zacchino, C. Somlai, I.G. Csizmadia, B. Penke, R.D. Enriz, Bioorg. Med. Chem. 14 (2006) 7604–7614.
[12] M. Zasloff, Curr. Opin. Immunol. 4 (1992) 3–7.
[13] T. Ganz, R.I. Lehrer, Pharmacol. Ther. 66 (1995) 191–205.
[14] J.A. Hoffman, F.C. Kafatos, C.A. Janeway Jr., R.A.B. Ezekowitz, Science 284 (1999) 1313–1318.
[15] R.E.W. Hancock, Lancet 349 (1997) 418–422.
[16] R.E.W. Hancock, A. Patrzykat, Curr. Drug Targets Infect. Disord. 2 (2002) 79–83.
[17] U. Langel (Ed.), Cell-penetrating Peptides: Processes and Applications, CRC Press, Boca Raton, FL, 2002.
[18] A. Joliot, C. Pernelle, H. Deagostini-Bazin, A. Prochiantz, Proc. Natl. Acad. Sci. U.S.A. 88 (1991) 1864–1868.
[19] D. Derossi, A.H. Joliot, G. Chassaing, A. Prochiantz, J. Biol. Chem. 269 (1994) 10444–10450.
[20] D. Derossi, S. Calvet, A. Trembleau, A. Brunissen, G. Chassaing, A. Prochiantz, J. Biol. Chem. 271 (1996) 18188–18193.
[21] G. Drin, M. Mazel, P. Clair, D. Mathieu, M. Kaczorek, J. Temsamani, Eur. J. Biochem. 268 (2001) 1304–1314.
[22] T. Letoha, S. Gaál, C. Somlai, Z. Venkei, H. Glavinas, E. Kusz, E. Duda, A. Czajlik, F. Peták, B. Penke, J. Pept. Sci. 11 (2005) 805–811.
[23] E. Dupont, A.H. Joliot, A. Prochiantz, in: U. Langel (Ed.), Cell-penetrating Peptides: Processes and Applications, CRC Press, Boca Raton, FL, 2002, pp. 23–51.
[24] S.A. Zachino, R.A. Yunes, V. Cechinel Filho, R.D. Enriz, V. Kouznetsov, J.C. Ribas, in: M. Rai, D. Mares (Eds.), Plant-derived Antimycotics: Current Trends and Future Prospects, Haworth Press, New York, 2003, pp. 1–47.
[25] M. Sortino, P. Delgado, S. Juárez, J. Quiroga, R. Abonía, B. Insuasty, M. Nogueras, L. Rodero, F.M. Garibotto, R.D. Enriz, S.A. Zacchino, Bioorg. Med. Chem. 15 (2007) 484–494.
[26] E.J. Ernst, E.E. Roling, R. Petzold, D.J. Keele, M.E. Klepser, Antimicrob. Agents Chemother. 46 (2002) 3846–3853.
[27] M. Schiffer, C.-H. Chang, F.J. Stevens, Protein Eng. 5 (1992) 213–214.
[28] T. Letoha, S. Gaál, C. Somlai, A. Czajlik, A. Perczel, B. Penke, J. Mol. Recognit. 16 (2003) 272–279.
[29] D.R. Ripoll, H.A. Scheraga, Biopolymers 27 (1988) 1283–1303.
[30] J.W. Ponder, TINKER – Software Tools for Molecular Design, User's Guide for Version 4.2, Washington University School of Medicine, 2004.
[31] E. Lindahl, B. Hess, D. van der Spoel, J. Mol. Model. 7 (2001) 306–317.
[32] D. van Der Spoel, A.R. van Buuren, E. Apol, P.J. Meulenhoff, D.P. Tieleman, A.L.T.M. Sijbers, B. Hess, K.A. Feenstra, E. Lindahl, R. van Drunen, H.J.C. Berendsen, GROningen Machine for Chemical Simulations, Department of Biophysical Chemistry, University of Groningen, Groningen, The Netherlands, 2002.
[33] M.F. Lensink, B. Christiaens, J. Vandekerckhove, A. Prochiantz, M. Rosseneu, Biophys. J. 88 (2005) 939–952.
[34] W. Kabsch, C. Sander, Biopolymers 22 (1983) 2577–2637.
[35] A. Czajlik, E. Meskó, B. Penke, A. Perczel, J. Pept. Sci. 8 (2002) 151–171.
[36] P. Politzer, D.G. Truhlar (Eds.), Chemical Applications of Atomic and Molecular Electrostatic Potentials, Plenum Press, New York, 1991.
[37] G. Náray-Szabó, G.G. Ferenczy, Chem. Rev. 95 (1995) 829–847.
[38] B. Christiaens, J. Grooten, M. Reusens, A. Joliot, M. Goethals, J. Vandekerckhove, A. Prochiantz, M. Rosseneu, Eur. J. Biochem. 271 (2004) 1187–1197.
[39] M.H. Lindberg, H. Biverstahl, A. Graslund, L. Maler, Eur. J. Biochem. 270 (2003) 3055–3063.
[40] C.E.B. Brattwall, P. Lincoln, B. Nordén, J. Am. Chem. Soc. 125 (2003) 14214–14215.
[41] J.A. Vila, D.R. Ripoll, H.A. Baldoni, H.A. Scheraga, J. Biomol. NMR 24 (2002) 245–262.
[42] P.E.G. Thorén, D. Persson, P. Isakson, M. Goksor, A. Onfelt, B. Nordén, Biochem. Biophys. Res. Commun. 307 (2003) 100–107.
[43] D.P. Kontoyiannis, E. Mantadakis, G. Samonis, J. Hosp. Infect. 53 (2003) 243–258.
[44] N. Singh, Lancet Infect. Dis. 3 (2003) 703–708.
[45] E. Kaiser, R.L. Colescott, C.D. Bossiuger, P.I. Cook, Anal. Biochem. 34 (1970) 595–598.
[46] Wayne (Ed.), second ed.NCCLS, National Committee for Clinical and Laboratory Standards, Method M27-A2, vol. 22, 2002, pp. 1–29.
[47] A. Liwo, A. Tempczyk, S. Oldziej, M.D. Shenderovich, V.J. Hruby, S. Talluri, J. Ciarkowski, S. Kasprzykowski, L. Lankiewicz, Z. Grzonka, Biopolymers 38 (1996) 157–175.
[48] G. Némethy, K.D. Gibson, K.A. Palmer, C.N. Yoon, G. Paterlini, A. Zagari, S. Rumsey, H.A. Scheraga, J. Phys. Chem. 96 (1992) 6472–6484.
[49] R.L. Williams, J. Vila, G. Perrot, H.A. Scheraga, Proteins: Struct., Funct., Genet. 14 (1992) 110–119.
[50] Z. Li, H.A. Scheraga, Proc. Natl. Acad. Sci. U.S.A. 84 (1987) 6611–6615.
[51] L. Piela, H.A. Scheraga, Biopolymers 26 (1987) S33–S58.
[52] N. Metropolis, A.W. Rosenbluth, M.N. Rosenbluth, A.H. Teller, E.J. Teller, Chem. Phys. 21 (1953) 1087–1091.
[53] M. Sidor, J. Wójcik, D. Pawlak, J. Izdebski, Acta Biochim. Pol. 46 (1999) 641–650.
[54] H.A. Scheraga, D.R. Ripoll, A. Liwo, C. Czaplewski, User Guide ECEPPAK and ANALYZE Programs, 1983.
[55] C.E. Kundrot, J.W. Ponder, F.M. Richards, J. Comput. Chem. 12 (1991) 402–409.
[56] M. Feig, J. Karanicolas, C.L. Brooks III, MMTSB Tool Set, MMTSB NIH Research Resource, The Scripps Research Institute, 2001. Available from:<http://feig.bch.msu.edu/mmtsb/Main_Page>.
[57] W.L. Jorgensen, D.S. Maxwell, J. Tirado-Rives, J. Am. Chem. Soc. 118 (1996) 11225–11236.
[58] E.K. Watkins, W.L. Jorgensen, J. Phys. Chem. A 105 (2001) 4118–4125.

[59] G.A. Kaminski, R.A. Friesner, J. Tirado-Rives, J. Phys. Chem. B 105 (2001) 6474–6487.
[60] H.J.C. Berendsen, J.P.M. Postma, W.F. van Gunsteren, J. Hermans, in: B. Pullman (Ed.), Intermolecular Forces, Reidel, Dordrecht, 1981, pp. 331–342.
[61] B. Hess, H. Bekker, H.J.C. Berendsen, J.G.E.M. Fraaije, J. Comput. Chem. 18 (1997) 1463–1472.
[62] S. Miyamoto, P.A. Kollman, J. Comput. Chem. 13 (1992) 952–962.
[63] H.J.C. Berendsen, J.P.M. Postma, W.F. van Gunsteren, A. DiNola, J.R. Haak, J. Chem. Phys. 81 (1984) 3684–3690.
[64] T. Darden, D. York, L. Pedersen, J. Chem. Phys. 98 (1993) 10089–10092.
[65] M.J. Frisch, G.W. Trucks, H.B. Schlegel, G.E. Scuseria, M.A. Robb, J.R. Cheeseman, J.A. Montgomery Jr., T. Vreven, K.N. Kudin, J.C. Burant, J.M. Millam, S.S. Iyengar, J. Tomasi, V. Barone, B. Mennucci, M. Cossi, G. Scalmani, N. Rega, G.A. Petersson, H. Nakatsuji, M. Hada, M. Ehara, K. Toyota, R. Fukuda, J. Hasegawa, M. Ishida, T. Nakajima, Y. Honda, O. Kitao, H. Nakai, M. Klene, X. Li, J.E. Knox, H.P. Hratchian, J.B. Cross, C. Adamo, J. Jaramillo, R. Gomperts, R.E. Stratmann, O. Yazyev, A.J. Austin, R. Cammi, C. Pomelli, J.W. Ochterski, P.Y. Ayala, K. Morokuma, G.A. Voth, P. Salvador, J.J. Dannenberg, V.G. Zakrzewski, S. Dapprich, A.D. Daniels, M.C. Strain, O. Farkas, D.K. Malick, A.D. Rabuck, K. Raghavachari, J.B. Foresman, J.V. Ortiz, Q. Cui, A.G. Baboul, S. Clifford, J. Cioslowski, B.B. Stefanov, G. Liu, A. Liashenko, P. Piskorz, I. Komaromi, R.L. Martin, D.J. Fox, T. Keith, M.A. Al-Laham, C.Y. Peng, A. Nanayakkara, M. Challacombe, P.M.W. Gill, B. Johnson, W. Chen, M.W. Wong, C. Gonzalez, J.A. Pople, Gaussian 03, Revision B.05, Gaussian, Inc., Pittsburgh, PA, 2003.
[66] P. Flükiger, H.P. Lüthi, S. Portmann, J. Weber, MOLEKEL 4.0, Swiss Center for Scientific Computing, Manno, Switzerland, 2000.